M. Kumari, Y. C. Sharma, Effect of doping with 'se' on structural, optical, electrical and thermoelectric properties of multilayers of $Bi_2Te_{2.7}Se_{0.3}/Sb_2Te_3$ to enhance thermoelectric performance,
Nanosystems: Physics, Chemistry, Mathematics, 2019, Volume 10, Issue 6, 686–693

NANOSYSTEMS: PHYSICS, CHEMISTRY, MATHEMATICS, 2019, 10 (6), P. 686–693

Effect of doping with 'se' on structural, optical, electrical and thermoelectric properties of multilayers of $Bi_2Te_{2.7}Se_{0.3}$ / Sb_2Te_3 to enhance thermoelectric performance

M. Kumari, Y. C. Sharma

Department of Physics, Vivekananda Global University, jagatpura, Jaipur-303012, Rajasthan, India

mjmanisha209@gmail.com

DOI 10.17586/2220-8054-2019-10-6-686-693

Selenium is known to be a semiconductor with many applications, and when it is doped in some chemical compounds, it changes the electrical properties of that compound which directly affect its thermoelectric performance. The present work is to synthesized multilayers of $Bi_2Te_{2.7}Se_{0.3}$ / Sb_2Te_3 by e-beam evaporation technique on glass substrate at room temperature. Prepared thin films were characterized by XRD and also study their electrical, optical and thermoelectrical properties to enhance the thermoelectric performance of Thermoelectric (TE) devices.

Keywords: thermoelectric, $Bi_2Te_{2.7}Se_{0.3}$, Sb_2Te_3, Figure of merit (ZT).

Received: 8 November 2019

Revised: 1 December 2019

1. Introduction

Thermoelectrics is a promising area for the conversion of any type of waste heat into electricity and suitable for power generation. The initial applications of thermoelectric materials was in spacecraft such as in Cassini, Voyager, and New Horizons [1, 2]. But now they have many other applications, such as in microcoolers and generators, in CCD technologies, and in infrared detectors. The unique property of thermoelectric devices for conversion of environmental waste heat introduced the elegant concept of harvesting energy from body. The source of energy from a body is thermal energy, which can be utilized and converted into self-powered wearable device [3]. To make a body-wearable device, the heat exchange from hot side to cold side is limited due to large inrefficient thermal resistances [4]. It should be remember that the material used for body-wearable device should have low thermal conductivity. Generally TE devices are not practically applicable, due to their low efficiency. Much research has been done in this field to increase the thermoelectric efficiency. The thermoelectric efficiency is directly dependent on a dimensionless quantity known as Figure of merit (ZT). Higher ZT values of lead to large thermoelectric efficiency. ZT directly depends on electrical conductivity and Seebeck coefficient and inversely proportional to thermal conductivity. The formula for figure of merit ZT= $S^2\sigma T/k$, where S is Seebeck coefficient, σ is electrical conductivity and k is thermal conductivity and T is absolute temperature. Much research has been done to increase the value of electrical conductivity and Seebeck coefficient by selecting an appropriate material. Bi_2Te_3 is most promising thermoelectric material showing good thermoelectric properties at room temperature, which can be used for many applications. Recent research on n-type Bi_2Te_3 alloys showing high ZT using nanostructuring [5–7], nonoelusions [8], texturing [9] and point defect engineering [10]. In many researches, it was found that n-type Bi_2Te_3 compounds have been shown high value of ZT but still they are not suitable for practical applications such as harvesting body heat due to non-optimized properties at room temperature. So, high value of ZT of a material with optimizing transport property at room temperature is required. To satisfy the above requirement recent researches are focused on decreasing lattice thermal conductivity by preparing superlattice structures. Recent enhancements have been done by Venkatasubramanian by fabricating superlattice structures of Bi_2Te_3 / Sb_2Te_3 with high figure of merit 2.4. For body heat harvesting applications, high value of σ and S with relatively low value of K is required at room temperature. So, as it is known that bismuth telluride has been shown to possess the best thermoelectric properties at room temperature and when it is doped with Sb, Se or with some other element it becomes an efficient thermoelectric material. Doping is a very common technique for the improvement in thermoelectric properties by increasing electrical conductivity and decreasing thermal conductivity as doping increased electron-phonon scattering. It has been reported that doping of elements like C, Sn, Pb, O, S, Se can increase the thermoelectric properties of Bi_2Te_3 [11–16]. Superlattice structures are focused on either a multilayered hetrojunction arrangement or by doping in one of the material to form a series of homojunctions [17]. It has been observed that appropriate amount of doping into a superlattice structure can make high performance thermoelectric module and can also develop new properties [18]. Thus, the present work is focused on the synthesis of multilayered $Bi_2Te_{2.7}Se_{0.3}$ / Sb_2Te_3 structures to fulfill the above requirement.

2. Experimental details

All the samples single layer $Bi_2Te_{2.7}Se_{0.3}$ and Sb_2Te_3 (50 nm) each, their bilayer $Bi_2Te_{2.7}Se_{0.3}$–Sb_2Te_3 (103 nm), 5 layers of thickness (510 nm) and 10 layers of total thickness (1024 nm) are fabricated on clean glass substrate by e-beam evaporation technique. The thickness of the films was measured from quartz crystal thickness monitor of vacuum coating unit. The $Bi_2Te_{2.7}Se_{0.3}$ and Sb_2Te_3 are purchased in the powder form from Sigma Company with 99.99% purity. Substrate were cleaned with acetone and dried at room temperature. All the thin films are deposited in a vacuum chamber under the pressure of $\sim 10^{-6}$ Pa with rate of evaporation for $Bi_2Te_{2.7}Se_{0.3}$ was $\sim$2Å/Sec. and for Sb_2Te_3 is $\sim$10Å/Sec. Structural properties are analyzed by XRD in Banasthali Vidyapeeth, Banasthali. The electrical properties like hall measurement, Carrier concentration, mobility, conductivity, sheet resistance and I–V measured were carried out through four probe method in MNIT, Jaipur. The optical properties were measured by LAMBDA 750 (Perkin Elmer) in MNIT, Jaipur to determine the band gap of the samples.

3. Results and discussion. Structural properties

3.1. X-RAY Diffraction (XRD)

The Xrd pattern of multilayers of $Bi_2Te_{2.7}Se_{0.3}$ / Sb_2Te_3 of different thicknesses from $\sim$(50–1000 nm) has been shown in Fig. 1. The main peaks observed in single layer $Bi_2Te_{2.7}Se_{0.3}$ are at 23.46°, 28.28° and 41.05°. There is no peak observed in Sb_2Te_3 which confirms its non- crystalline or amorphous nature. As thicknesses of the samples increases more number of peaks is generated at angles 50.44°, 64.86° and 66.20°, which cannot be observed in single layer $Bi_2Te_{2.7}Se_{0.3}$. The intensity of the peaks is increased, which confirms that crystallinity of the thin films increases as number of alternate layer increases. The Xrd patterns of the multilayer structure of $Bi_2Te_{2.7}Se_{0.3}$ / Sb_2Te_3 are well matched with Xrd pattern in paper of [19].

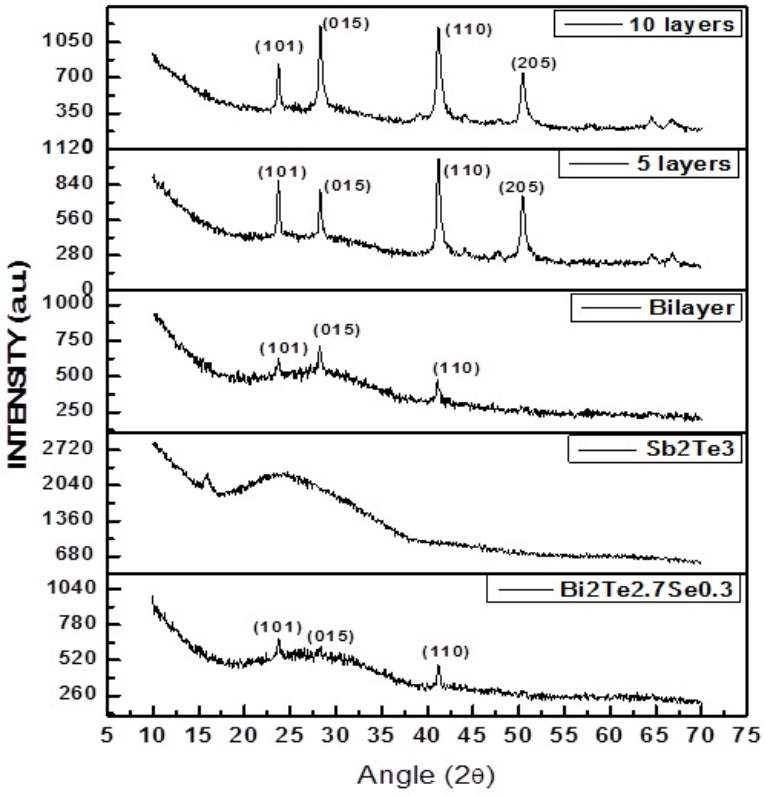

FIG. 1. XRD pattern of multilayers of $Bi_2Te_{2.7}Se_{0.3}$ / Sb_2Te_3 at room temperature

3.1.1. Grain Size. The grain size of the samples of different thicknesses can be calculated using Scherer's formula:

$$D = \frac{k\lambda}{\beta \cos\theta} \tag{1}$$

The calculated structural parameters Full width at half maxima (FWHM), Grain size (D), microstrain (ε), and dislocation density (δ) for alternate layers of $Bi_2Te_{2.7}Se_{0.3}$ / Sb_2Te_3 of various thicknesses ranging from (50–1000 nm) for (0 1 5) orientation have been shown in Table 1.

TABLE 1. The calculated structural parameters, Full width at half maxima (FWHM), Grain size (D), microstrain (ε), and dislocation density (δ) for alternate layers of $Bi_2Te_{2.7}Se_{0.3}$ / Sb_2Te_3 for (0 1 5) orientation

Samples	FWHM β^0	Grain Size(D) (nm)	Strain $(\varepsilon \cdot 10^{-4})$ (lines^{-2}m^{-4})	Dislocation density $(\delta \cdot 10^{13})$ (lines/m^2)
$Bi_2Te_{2.7}Se_{0.3}$ (50 nm)	0.2172	37.76	9.18	70.13
Sb_2Te_3(53 nm)	0.492	16.29	21.26	376.84
Bilayer (103 nm)	0.1855	44.28	7.84	51.00
5 layers (510 nm)	0.2052	39.94	8.67	62.68
10 layers (1024 nm)	0.2879	28.47	12.17	123.37

Where D is the grain size, k is the shape factor (0.94), λ is the wave length of X-ray source (1.5406 Å), θ is the Bragg's angle and β is full width at half maxima.

3.1.2. Microstrain. The microstrain (ε) is developed in thin films is the root mean square of variations in lattice parameters. It can be calculated from the relation:

$$\varepsilon = \frac{\beta \cos\theta}{4} \tag{2}$$

3.1.3. Dislocation density. Dislocation in Xrd is an imperfection in crystal which occurs due to misregistry of lattice in one part with another part of the lattice [17]. The dislocation density (δ) is the length of dislocation lines per unit volume of crystal and it can be determined by the relation:

$$\delta = \frac{1}{D^2} \tag{3}$$

3.2. Scanning Electron Microscopy (SEM)

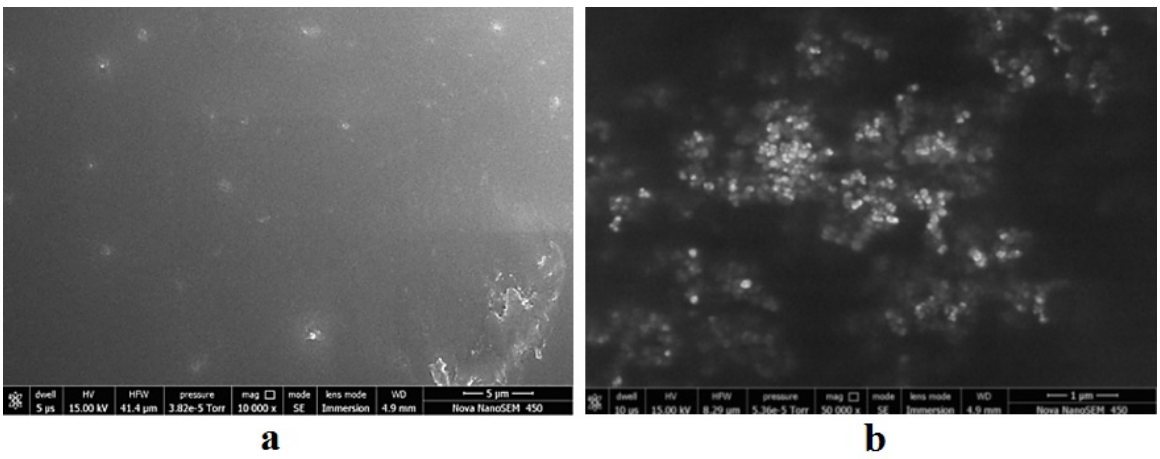

FIG. 2. SEM images of (a) $Bi_2Te_{2.7}Se_{0.3}$ (b) Sb_2Te_3

The SEM images of single layer of $Bi_2Te_{2.7}Se_{0.3}$ and Sb_2Te_3 are shown in Fig. 2. The average grain size from SEM analysis for $Bi_2Te_{2.7}Se_{0.3}$ and Sb_2Te_3 sample is $\sim$44 nm and 20 nm. It was observed that crystallinity and grain size increase from single layer $Bi_2Te_{2.7}Se_{0.3}$ to bilayer. These results are in good agreement with XRD results.

4. Electrical properties

4.1. I–V Measurements

Figure 3 shown the I–V behavior of multilayers of $Bi_2Te_{2.7}Se_{0.3}$ / Sb_2Te_3 at room temperature. The current is flowing through the samples in milliampere range. The graph shows that slope of the curves increase with thicknesses which determine the conductivity of the sample. It is also been observed that single layer $Bi_2Te_{2.7}Se_{0.3}$ and Sb_2Te_3 show almost linear behavior but a nonlinear behavior is observed as thickness increases up to 5 layers. The semiconducting behavior of the curves increases with thickness which shows that decreasing conductivity.

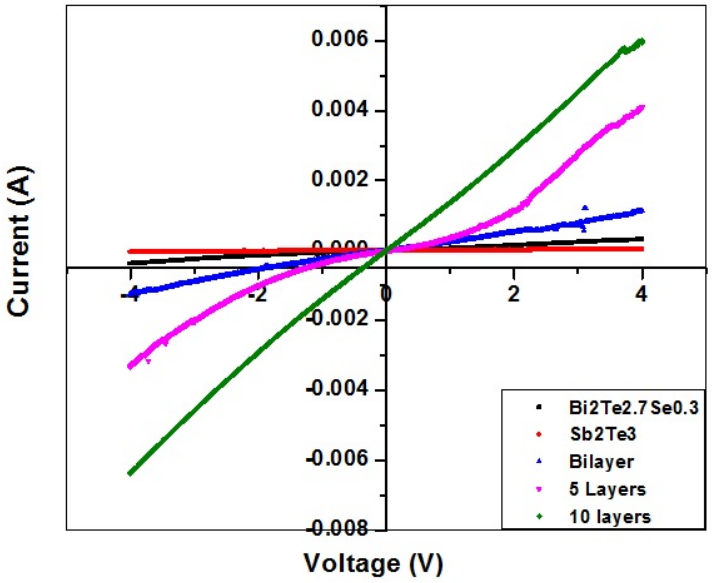

FIG. 3. I–V curves of multilayers of$Bi_2Te_2Se_{0.3}$ / Sb_2Te_3 at room temperatures

4.2. Hall measurements

Table 2 shows the measured Electrical conductivity, Sheet resistance, Bulk carrier concentration, Hall coefficient, mobility and magneto resistance of the Se doped $Bi_2Te_{2.7}Se_{0.3}$, Sb_2Te_3, Bilayer, 5 layers, 10 layers at room temperature. It has been observed that highest electrical conductivity is examined for single layer $Bi_2Te_{2.7}Se_{0.3}$ of $2.43\cdot(10^2\ \Omega\cdot m)^{-1}$ and decreases as thickness of alternate layers increases.

TABLE 2. Represents Electrical properties of multilayers of $Bi_2Te_{2.7}Se_{0.3}$ / Sb_2Te_3

Samples	Bulk conc. (10^{21})	Sheet resistance ($10^3\ \Omega$)	Conductivity ($10^2\ \Omega\cdot cm)^{-1}$	Hall coefficient, R_H ($10^{-3}cm^3/C$)	Mobility, μ ($cm^2/V\cdot sec.$)	Magneto resistance (10^{-1})
$Bi_2Te_{2.7}Se_{0.3}$	1.38	0.815	2.43	4.58	1.10	0.56
Sb_2Te_3	2.64	1.00	1.87	2.35	4.58	16100
Bilayer	0.67	0.984	0.99	9.23	1.58	1.11
5 layers	0.13	0.207	0.95	3.42	4.30	1.93
10 layers	0.12	0.152	0.64	2.53	5.77	0.50

In order to examine the electronic transport properties, Bulk carrier concentration (n), mobility (μ) and Hall coefficient (R_H) were measured at room temperature. The sign of Hall coefficient was positive for all the samples. It shows that main electrical charge carriers are hole and showing p-type semiconducting behavior. The maximum value of hall coefficient $9.23\cdot(10^{-3}\ cm^3/C)$ is found for bilayer sample but decreases as thickness of the sample was further

increases. A high value of carrier concentration of (10^{21}) is achieved for all the samples and decrease with thickness. Mobility increases as the number of alternate layers increases. Maximum mobility 5.77 (cm^2/V·sec.) and minimum carrier concentration $0.12 \cdot 10^{21}$ is found to be for 10-layered sample.

Magneto resistance is also an important parameter to study in the field of thermoelectricity which is the tendency of material to change its electrical resistance on the application of eternal magnetic field. In multilayer system tunnel junctions are formed that's why the term giant magnetoresistance (GMR) is used. A high GMR is achieved for single layered Sb_2Te_3 which shows that maximum change in resistance is observed for Sb_2Te_3 on the application external magnetic field.

5. Optical properties

In optical properties, absorbance spectra of all the samples with different thickness were recorded using UV-VIS-NIR double beam spectrometer in the range of (200–1100) nm. Fig. 4 show the optical absorption spectra of single layer $Bi_2Te_{2.7}Se_{0.3}$, Sb_2Te_3 and Bilayer sample. It is obvious that absorption increases with thickness. But, as the thickness increases to 5 or 10 layers, the absorbance pattern was not clearly observed. Because as thickness of the sample is large, the absorbance is greater and only some part of the light will be transmitted through the sample. It is clearly observed from the graph that low absorbance is found in 300–350 nm region which lies in visible region. For all the three samples maximum absorbance was found only at one position which confirms the uniformity of the sample.

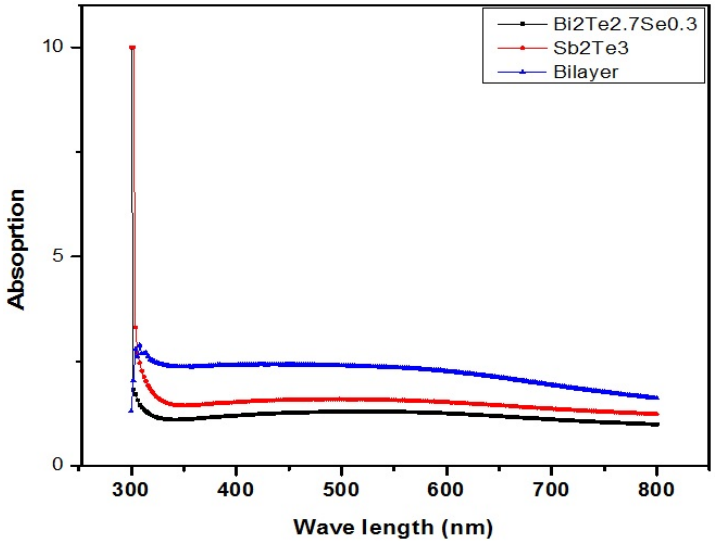

FIG. 4. Show the optical absorption spectra of $Bi_2Te_{2.7}Se_{0.3}$, Sb_2Te_3 and Bilayer sample

The absorption coefficient (α) is determined from transmittance measurements using relation [20]:

$$\alpha = \frac{2.303}{d} \log_{10} \frac{1}{T} \tag{4}$$

where T is transmittance and d is the thickness of the film.

The electronic transition between valence band and conduction band can also be calculated from absorption coefficient using:

$$\alpha = A(h\nu - E_g)^p \tag{5}$$

where A is constant, E_g is the optical band gap, $h\nu$ is incident photon energy and P has discrete values like $\frac{1}{2}$, $\frac{3}{2}$, $\frac{4}{2}$,... etc., depending upon the transition. For direct and allowed transition $P = \frac{1}{2}$, in direct but forbidden case $P = \frac{3}{2}$, and for indirect and allowed transition $P = 2$ and for forbidden case it will be 2 or more. The band gap is determined by extrapolation on x-axis in curve between $(\alpha h\nu)^2$ and $h\nu$. The optical band gap has been determined for different thickness shown in Fig. 5. It has been shown that band gap increases with thickness up to the bilayer and then decreases for 5-layered sample. The graphs show the direct and allowed transitions. These values of band gaps E_g for $Bi_2Te_{2.7}Se_{0.3}$, Sb_2Te_3. Bilayer and layers are 1.34, 1.72, 1.56, 1.22 eV. The variation in band gaps is due to variation

in grain size and dislocation density. As dislocation density is high resulting in high band gap of a semiconductor because presence the separation distance of dislocations are greater than interatomic distance [21]. The results are in good agreement with the results of XRD shown in Table 2.

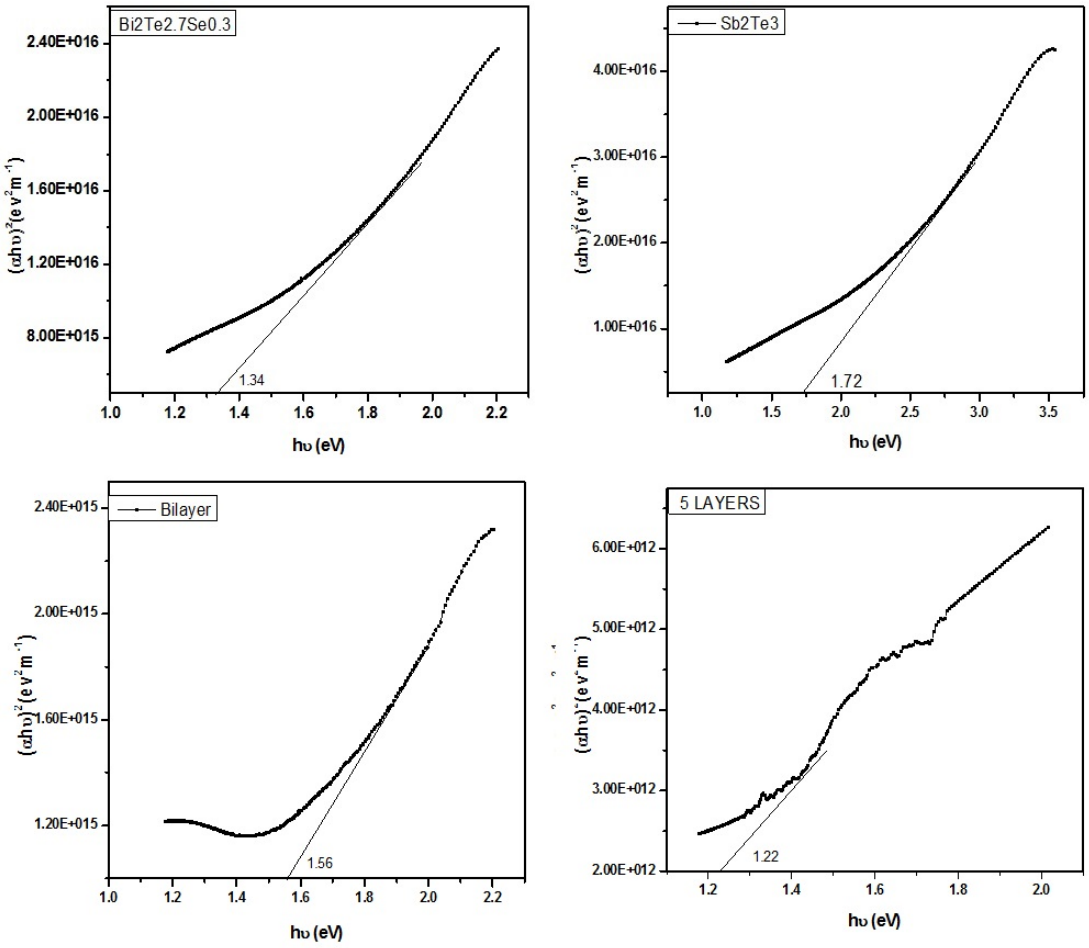

FIG. 5. Band gaps of $Bi_2Te_{2.7}Se_{0.3}$–Sb_2Te_3 thin films

5.1. Thermoelectric Properties

TABLE 3. Represents the Thermoelectrical properties of multilayers of Bi_2Te_3–Sb_2Te_3

Sample details	Seebeck coefficient S (μV/K)	Resistivity ρ ($\mu\Omega$·m)	Power factor (10^{-3}·W/m·K^2)
$Bi_2Te_{2.7}Se_{0.3}$	−87	41.15	0.183
Sb_2Te_3	210	53.4	0.825
Bilayer	238	101.0	0.560
5 layers	167	105.2	0.265
10 layers	123	156.2	0.096

In thermoelectric measurements, Seebeck coefficients of the samples were measured at room temperature. The Seebeck coefficient, resistivity and power factor of the samples are shown in Table 3. The negative value of Seebeck

coefficient for single layer $Bi_2Te_{2.7}Se_{0.3}$ shows n-type charge carrier and positive values for other samples show p-type charge carriers. The results have been shown that maximum Seebeck coefficient is achieved for bilayer sample but Power factor is maximum for Sb_2Te_3. The variations in Seebeck coefficient and power factor are shown in Fig. 6.

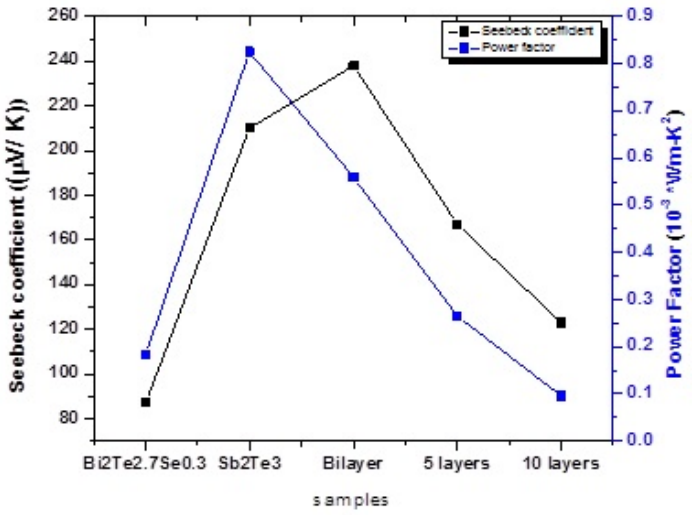

FIG. 6. Seebeck coefficient and power factor of $Bi_2Te_{2.7}Se_{0.3}$–Sb_2Te_3 thin films

6. Conclusion

The multilayered thin films of $Bi_2Te_{2.7}Se_{0.3}$ / Sb_2Te_3 variable thickness from (50–1000) nm were deposited on glass substrate at room temperature by using e-beam evaporation technique. The effect of thickness on structural, electrical and optical properties was studied. XRD studies indicates that the single layer $Bi_2Te_{2.7}Se_{0.3}$ thin film showed polycrystalline nature with preferred orientation along (0 1 5) plane, whereas the single layer Sb_2Te_3 show non crystalline or amorphous nature. Also, as the number of layers increases, the intensity of the planes also increases, which shows that crystallinity increases with thickness. The grain size also increases from single layer to bilayer, but after that, it decreases as the number of layers further increases. SEM analysis shows that single layer $Bi_2Te_{2.7}Se_{0.3}$ and Sb_2Te_3 have average grain size around 44 nm and 20 nm respectively. Results of I–V curve shows that slope increases with thickness and in electrical properties conductivity and charge carrier concentration decreases, whereas mobility increases with thickness. The optical properties show that absorption of all the samples were near visible region and optical transition was found to be direct and allowed. The energy band gap varies with thickness and lies between (1.34–1.72) eV. The maximum band gap was found for Sb_2Te_3. In thermoelectric measurements, the maximum Seebeck was found for Bilayer sample, but the power factor was maximum for single layer Sb_2Te_3.

References

[1] Nozariasbmarz A., Krasinski J.S., Vashaee D., N-Type Bismuth Telluride Nanocomposite Materials Optimization for Thermoelectric Generators in Wearable Applications. *Materials*, 2019, **12**(9), P. 1529.

[2] Schmidt G.R., Sutliff T.J., Dudzinksi L.A. Radioisotope Power: A Key Technology for Deep Space Exploration. In: Singh N., editor. Radioisotopes-Applications in Physical Science. InTech, London, UK, 2011. p. 419.

[3] Bell L.E. Cooling, Heating, Generating Power, and Recovering Waste Heat with Thermoelectric Systems. *Science*, 2008, **321**, P. 1457.

[4] Suarez F., Nozariasbmarz A., Vashaee D., Öztürk M.C. Designing thermoelectric generators for self-powered wearable electronics. *Energy Environment Science*, 2016, **9**, P. 2099–2113.

[5] Yan X., Poudel B., Ma Y., Liu W.S., Joshi G., Wang H., Lan Y.C., Wang D.Z., Chen G., Ren Z.F. Experimental studies on anisotropic thermoelectric properties and structures of n-type $Bi_2Te_{2.7}Se_{0.3}$. *Nano Lett.*, 2010, **10**, P. 3373.

[6] Liu W.S., Zhang Q., Lan Y., Chen S., Yan X., Zhang Q., Wang H., Wang D., Chen G., Ren Z. Thermoelectric Property Studies on Cu-Doped n-type $Cu_xBi_2Te_{2.7}Se_{0.3}$ nanocomposites. *Adv. Energy Mater*, 2011, **1**, P. 577.

[7] Hong M., Chasapis T.C., Chen Z.G., Yang L., Kanatzidis M.G., Snyder G.J., Zou J. n-type $Bi_2Te_{3-x}Se_x$ Nanoplates with Enhanced Thermoelectric Efficiency Driven by Wide Frequency Phonon Scatterings and Synergistic Carrier Scatterings. *ACS Nano*, 2016, **10**, P. 4719.

[8] Song S., Wang J., Xu B., Lei X., Jiang H., Jin Y., Zhang Q., Ren Z. Thermoelectric properties of n-type $Bi_2Te_{2.7}Se_{0.3}$ with addition of nano-ZnO:Al particles. *Material Research Express*, 2014, **1**, P. 035901.

[9] Hu L.P., Liu X.H., Xie H.H., Shen J.J., Zhu T.J., Zhao X.B. Improving thermoelectric properties of n-type bismuth–telluride-based alloys by deformation-induced lattice defects and texture enhancement. *Acta Mater.*, 2012, **60**, P. 4431.

[10] Hu L., Zhu T., Liu X., Zhao X. Point Defect Engineering of High-Performance Bismuth-Telluride-Based Thermoelectric Materials. *Adv. Funct. Mater.*, 2014, **24**, P. 5211–5218.
[11] Tortoich R., Choi J.W. Inkjet. Printing of Carbon Nanotubes. *Nanomaterials*, 2013, **3**(3), P. 453.
[12] Fukuda K., Someya T. Recent Progress in the Development of Printed Thin Film Transistors and Circuits with High Resolution Printing Technology. *Advanced Materials*, 2016, **29**, P. 1–22.
[13] Morgan K.A. et al. *Tuneable sputtered films by doping for wearable and flexible thermoelectrics*. Presented at Materials Research Society Fall, Boston, USA, 2017.
[14] Zhou Y., Li L., Tan Q., Li J.-F. Thermoelectric properties of Pb-doped bismuth telluride thin films deposited by magnetron sputtering. *Journal of Alloys and Compounds*, 2014, **590**, P. 362.
[15] Fan P. et al. Low-cost flexible thin film thermoelectric generator on zinc based thermoelectric materials. *Applied Physics Letters*, 2015, **106**, P. 073.
[16] Zheng S.H. et al. Using high thermal stability flexible thin film thermoelectric generator at moderate temperature. *Applied Physics Letters*, 2018, **112**, P. 163.
[17] Albuquerque E.L., Michael Cottam, Surface Plasmon- and Phonon-Polaritons. In book: Polaritons in Periodic and Quasiperiodic Structures, P. 65–87.
[18] Il-Ho Kim, Soon-Mok Choi, Won-Seon Seo, Dong-Ik Cheong, Hyung Kang. Thermoelectric properties of cu-dispersed $Bi_2Te_{2.7}Se_{0.3}$ nanocomposites, 18th international conference on composite materials, Korea.
[19] Sathyamoorthy R., Dheepa J. Structural characterization of thermally evaporated Bi_2Te_3 thin films. *Journal of Physics and Chemistry of Solids*, 2007, **68**, P. 111.
[20] Dheepa J., Sathyamoorthy R., Subbarayan A. Optical properties of thermally evaporated Bi_2Te_3 thin films. *Journal of Crystal Growth*, 2005, **274**, P. 100–105.
[21] Deshmukh G.D., Patil S.M., Patil S.S., Pawar P.H. Effect of Film Thickness on Structural and Optical Properties of Bi_2Te_3 Thin Films. *Journal of Chemical, Biological and Physical Sciences*. 2015, **5**, P. 2769.